Journal of Dental Sciences 21 (2026) 541–550

Available online at www.sciencedirect.com

ScienceDirect

journal homepage: www.e-jds.com

Original Article

Apoptosis-inducing factor mitochondria-associated 2 (AIFM2) *promotes tumor progression and predicts poor prognosis in oral squamous cell carcinoma*

Chung-Hsien Chou [a], Kuo-Wei Chang [a,b,c], Wan-Wen Hung [a], Miao-An Wei [a], Chung-Ji Liu [a,c,d], Shu-Chun Lin [a,b,c*]

[a] *Institute of Oral Biology, College of Dentistry, National Yang Ming Chiao Tung University, Taipei, Taiwan*
[b] *Department of Dentistry, College of Dentistry, National Yang Ming Chiao Tung University, Taipei, Taiwan*
[c] *Department of Stomatology, Taipei Veterans General Hospital, Taipei, Taiwan*
[d] *Department of Stomatology, Taipei Mackay Memorial Hospital, Taipei, Taiwan*

Received 5 November 2025; Final revision received 7 November 2025
Available online 22 November 2025

KEYWORDS
AIFM2;
Head and neck carcinoma;
Oral carcinoma;
Prognosis

Abstract *Background/purpose:* Head and neck squamous cell carcinoma (HNSCC), including oral squamous cell carcinoma (OSCC), remains a major malignancy with limited therapeutic efficacy. Apoptosis-inducing factor mitochondria-associated 2 (AIFM2), also known as ferroptosis suppressor protein 1, regulates ferroptosis and tumor progression. This study investigated the oncogenic function, clinical relevance, and regulation of AIFM2 in OSCC.
Materials and methods: Transcriptomic data from TCGA HNSCC and in-house OSCC RNA-Seq datasets were analyzed to assess AIFM2 expression and its association with clinicopathological features and outcomes. Functional assays evaluated the effects of AIFM2 knockdown or overexpression on OSCC cell proliferation, migration, invasion, and therapeutic response. MicroRNAs targeting AIFM2 were identified through bioinformatics, luciferase reporter, and mimic assays. A Light Gradient Boosting Machine (LGBM) model was used for prognostic prediction.
Results: AIFM2 overexpression was associated with advanced stage, poor tumor differentiation, and unfavorable survival in HNSCC/OSCC. AIFM2 knockdown suppressed, whereas its overexpression enhanced, OSCC cell proliferation, migration, and invasion, while exerting minimal effects on cisplatin, palbociclib, or cold atmospheric plasma sensitivity. miR-32-5p and miR-432-5p directly targeted AIFM2 and were downregulated in tumors. AIFM2-associated

* Corresponding author. Institute of Oral Biology, College of Dentistry, National Yang Ming Chiao Tung University, No. 155, Section 2, LiNong St, 11211, Taipei, Taiwan.
E-mail address: shuchun@nycu.edu.tw (S.-C. Lin).

https://doi.org/10.1016/j.jds.2025.11.007

transcripts were enriched in pathways related to oxidative stress, lipid metabolism, and E2F targets. The LGBM-derived AIFM2 gene signature demonstrated strong prognostic predictive power.
Conclusion: AIFM2 acts as an oncogenic driver in OSCC, regulated by tumor-suppressive miR-32-5p and miR-432-5p, and serves as a potential prognostic biomarker and therapeutic target.

Introduction

Oral squamous cell carcinoma (OSCC) is one of the highly prevalent malignancies in the world, accounting for a significant proportion of head and neck cancers (HNSCC).[1–4] Despite advances in treatment, the therapeutic efficacy against HNSCC/OSCC is still a challenging issue. Ferroptosis is an iron-dependent cell death,[5] characterized by the excessive redox species (ROS) accumulation generated by the Fenton reaction, which causes lipid peroxidation, the abnormalities of mitochondria, and the activation of the death cascade.[5–11] Recent studies showed that the activation of ferroptosis regulators can enrich the therapeutic outcomes of HNSCC/OSCC.[12,13] We have demonstrated that cold atmospheric plasma (CAP) irradiation induced the death of OSCC cells, including the ferroptotic death.[14]

Previous studies revealed that apoptosis-inducing factor mitochondria-associated 2 (AIFM2) is a pro-apoptotic factor, which is downregulated by p53.[15–17] As AIFM2 harbors an oxidoreductase box, membrane-anchored AIFM2 catalyzes the reduction of CoQ10 to CoQ10H2, which in turn prevents lipid peroxidation and restricts the ferroptotic process.[18,19] As a ferroptosis suppressor protein, AIFM2 has also been named FSP1 accordingly. Inhibition of AIFM2 significantly enhanced ferroptosis sensitivity in multiple cancer cell lines.[20] The complicated roles of AIFM2 in the tumor process and therapy resistance have been revealed in recent studies.[15,21–27] AIFM2 expression promotes tumor metastasis in hepatocellular carcinoma.[24] Knockdown of AIFM2 attenuated the stemness and oncogenicity of drug-resistant tongue cancer cells.[26] However, knockout of AIFM2 reverted the oncogenicity being repressed in prostate cancers.[15] Although database analysis unveiled the AIFM2 upregulation in HNSCC,[26] the oncogenic activity of HNSCC/OSCC following AIFM2 expression has not yet been comprehensively defined. Comprehensive assessment is required to specify the clinicopathological values of AIFM2 in HNSCC/OSCC.

miRNAs play important roles in repressing targets transcript and modulating cellular physiology. Oncogenic miRNAs significantly upregulated in HNSCC/OSCC tissues promote tumor cells' growth, migration, invasion, and xenografic growth by targeting suppressor networks.[2,28–30] On the contrary, suppressor miRNAs downregulated in tumors may signify a favorable therapeutic outcome.[31–35] CAP irradiation downregulated oncogenic miRNAs and upregulated suppressor miRNAs, which may underlie the death of OSCC cells.[14] So far, miR-150-5p, miR-1228, and miR-3622b-3p, which directly target the 3′UTR of AIFM2 transcript and downregulate AIFM2 expression, have been reported in diseases.[15,23,25,36] The epigenetic modulation of AIFM2 through other miRNAs in HNSCC/OSCC requires elucidation.

This study demonstrates that AIFM2 is a prognostic predictor of HNSCC/OSCC. Although AIFM2 mediates the increased proliferation, migration, and invasion of HNSCC/OSCC cells, the influence of AIFM2 expression on therapeutic responses could be limited in this malignancy. Our previous study has stratified that suppressor miRNA miR-432-5p targeted VGF to modulate the OSCC progression.[3] This study also identifies that miR-32-3p and miR-432-5p are downregulated in HNSCC and they target AIFM2.[3,33–35] To abrogate AIFM2 function would validate HNSCC/OSCC interception.

Materials and methods

Cells and reagents

Normal oral keratinocyte NOK immortalized with hTERT, and HNSCC cell lines SAS, OECM1, FaDu, OC3, OC4, Cal27, and SCC25 were cultured as previously described.[37] Cisplatin (CDDP), Palbociclib, Doxycycline (Doxy), and other unspecified reagents were purchased from Sigma–Aldrich (St Louise, MO, USA). TransFectin lipid reagent (BioRad, Hercules, CA, USA) was used for transfection.

HNSCC/OSCC transcriptional signatures

The transcriptomic data and corresponding clinical information of HNSCC tumor and normal tissues were obtained from The Cancer Genome Atlas (TCGA; https://portal.gdc.cancer.gov/) (Table S1). Transcriptomic data and RNA samples from OSCC patients were collected after obtaining written informed consent (Table S2). This study was approved by the Institutional Review Board (IRB approval number: 18MMHIS187e). High-quality RNA samples were subjected to RNA sequencing (RNA-Seq). Transcript abundance was quantified using transcripts per million (TPM), while miRNA expression levels in TCGA dataset were normalized as reads per million (RPM).

Assays for proliferation, wound healing, invasion, and dose–response

Cell proliferation was analyzed using the trypan blue exclusion assay. Wound healing assay was used to measure the cell migration.[1] For the invasion assays, 50 μl of 10 %

Matrigel (BD Biosciences, San Jose, CA, USA) was used to coat Transwell membrane, and then cells were seeded onto the Matrigel-coated Transwell. After incubating cells at 37 °C for 48 h, the Transwell membranes were fixed and stained with Hoechst 33258. Images of the invaded cells were captured using a fluorescence microscope. Cell growth in the wound healing and invasion assays was arrested by treatment with 1 μM hydroxyurea. The dose response curves and IC_{50} were generated using MTT assay.[3]

miRNA mimics and siRNAs

miRNA mimics and the miRNA Scr were purchased from Applied Biosystems (Waltham, MA, USA). The si-AIFM2 oligonucleotide and si-RNA-A scramble control oligonucleotide were purchased from Santa Cruz Biotech (Santa Cruz, CA, USA) (Table S3). They were used following our previously established protocols.[1,2]

qPCR analysis

Total RNA was isolated from using TriPure Isolation Reagent (Roche, Basel, Switzerland), and was reversely transcribed. The AIFM2 mRNA expression was analyzed using quantitative polymerase chain reaction (qPCR), probe (Cat no. Hs01097300_m1), and reagents supplied by Applied Biosystems.[1,2] The resulting information was analyzed using the $-\Delta\Delta C_t$ method, and values were calculated relative to GAPDH analyzed using probe (Cat No. Hs00266705_g1).

Western blot analysis

Aliquots of cell lysate were subjected to Western blot analysis according to protocols previously published.[1] The primary antibodies for detecting oncogenic kinases, ferroptotic proteins and green fluorescence protein (GFP) are listed in Table S4. Signals were revealed by Western Lightning Chemiluminescence Reagent Plus kit (Thermo Scientific, Waltham, MA, USA) and detected using a FUJIFILM LAS-4000 mini luminescent image analyzer (GE Life Sciences, Piscataway, NJ, USA). The signals of tested proteins were normalized against GAPDH or α-tubulin to designate the expression level.

Plasmid construction and stable cell subclone establishment

The amplicon of the AIFM2 coding sequence (CDS) was digested with restriction enzymes, then cloned into the pcDNA3.1(−) (va) plasmid to enable transient overexpression (oe) (Table S5). A multiple cloning site (MCS) fragment was engineered into the TetOn lentiviral vector (pCW57.1, plasmid #41393, Addgene, Watertown, MA, USA) to generate a modified vector designated TetOn-MCS. The AIFM2 CDS amplicon was ligated into the TetOn-MCS vector (Table S5). Stable AIFM2-expressing cell subclones were established through lentiviral infection followed by blasticidin selection and were designated as AIFM2 OE (VA-related). In parallel, stable GFP OE cell subclones were generated to verify Doxy-induced expression of GFP (Table S5). The plasmids for AKT, ERK, and p38 activation are those we previously used.[14] The signals were activated by transient OE in relation to the control vector.

Construction of miRNA reporters

A 395-bp amplicon of the head (H) part and a 579-bp amplicon of the tail (H) part of the 3′ untranslated region (3′UTR) sequence in AIFM2, which encompasses the predicted targeted sites of tested miRNAs, were cloned into the pMIR-REPORT™ Luciferase vector (Life Technologies, Grand Island, NY, USA) to generate reporters (Table S6). Firefly luciferase activity, after normalizing to transfection efficiency, represented reporter activity. Following the treatment with miRNA mimics, the fold change of reporter activity is determined by normalizing to Scr treatment and the vector alone reporter (VAR) activity.

Bioinformatic algorithms

In silico searches of prediction modules specified potential targeting miRNAs overlapped, including Diana, microRNA, mirDIP, miRBD, or TargetScan. Venn diagram was used for illustrating the overlaps. The DESeq 2 program and volcano plot were used to illustrate the differentially expressed genes in TCGA HNSCC dataset. Gene set enrichment analysis (GSEA) algorithm and bubble plots annotated the enrichment of gene sets associated with AIFM2 expression. The hazard ratio of patients being defined by a regression model was achieved from a platform established in our laboratory.[38] The prognostic signatures were analyzed using a Light Gradient Boosting Machine (LGBM) model (https://lightgbm.readthedocs.io).[39] The prediction accuracy of the patient survival was evaluated by time-dependent receiver operating characteristic curve (ROC) mode.

Statistical analyses

The data were presented as means ± SE. Mann–Whitney tests, unpaired t-tests, two-way ANOVA tests, and Kaplan–Meier survival analysis were used to compare the differences between the various groups of results. A *P* value of less than 0.05 was considered significantly different.

Results

High AIFM2 expression defines the unfavorable HNSCC/OSCC prognosis

Analysis of the TCGA HNSCC dataset revealed a progressive increase in AIFM2 expression corresponding to tumor stage severity and the presence of lymphovascular invasion (Fig. 1A, Table S1). In both HNSCC and OSCC cohorts, higher histolopathologic grades were associated with elevated AIFM2 expression. Moreover, tumor site was significantly correlated with AIFM2 expression (Fig. 1A and B; Table S1 and Table S2). Notably, heavy smokers, defined as patients with tobacco consumption above the median pack-year value, exhibited higher AIFM2 expression in their

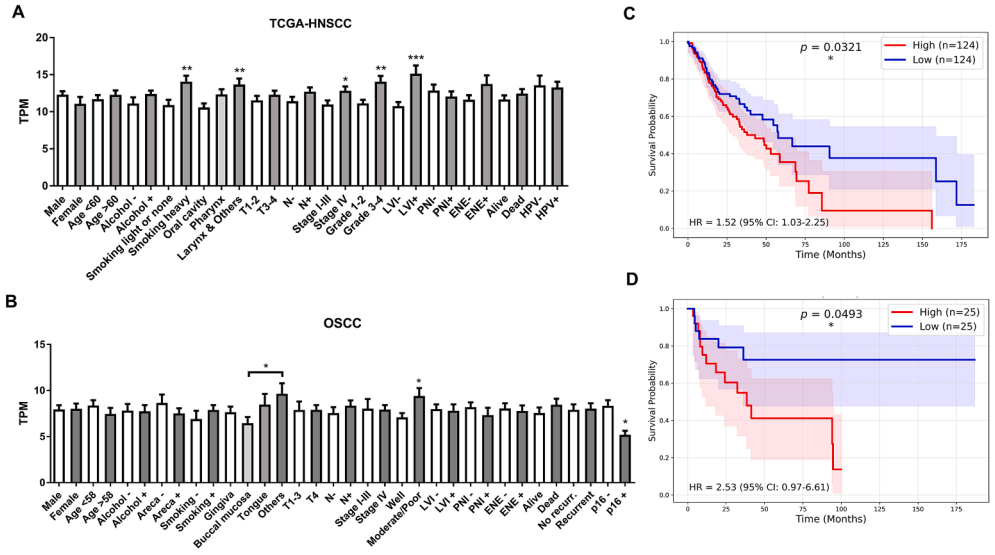

Figure 1 The association between AIFM2 expression and clinicopathological states in HNSCC/OSCC. (A, C) HNSCC. (B, D) OSCC. (A, B) Clinicopathological variants as related to AIFM2 expression. (C, D) Kaplan–Meier survival curve. T, tumor size; N, nodal metastasis; PNI, perineural invasion; LVI, lymphovascular invasion; ENE, extranodal extension; TPM, transcripts per million. *, **, and ***, $P < 0.05$, $P < 0.01$, and $P < 0.001$, respectively.

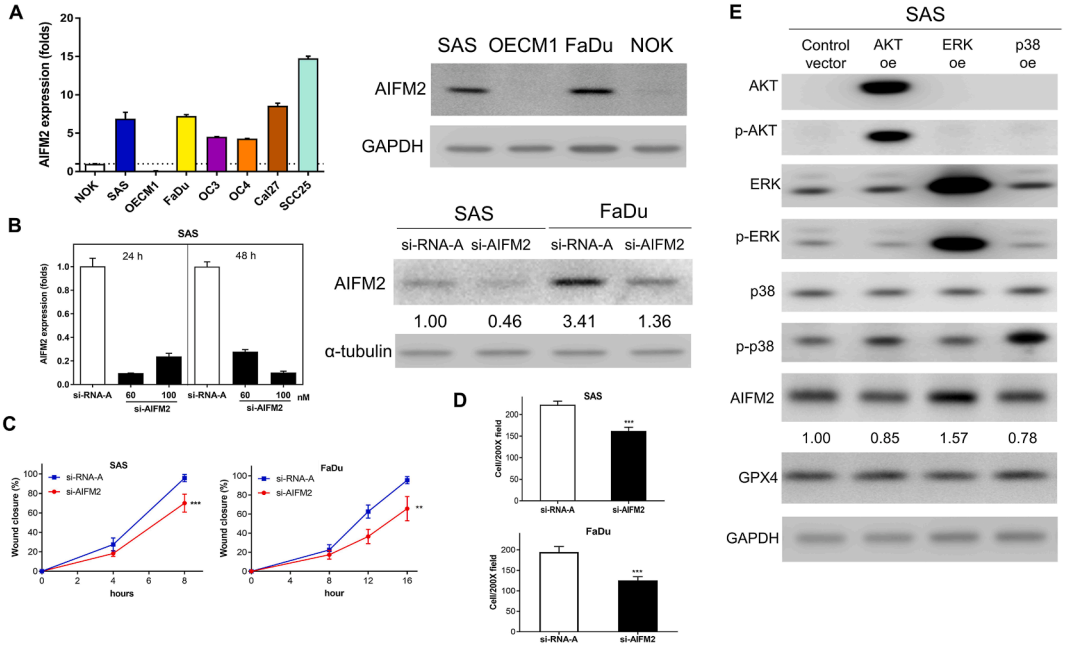

Figure 2 The AIFM2 expression in cell lines. (A) NOK and HNSCC/OSCC cell lines. Lt, qPCR analysis reveals the higher AIFM2 expression in cancer cell lines relative to NOK, except for OECM1. Rt, Western blot analysis reveals the AIFM2 expression in SAS and FaDu cells. NOK and OECM1 exhibits scanty and absent AIFM2 expression. (B) AIFM2 knockdown. Cells are treated with si-AIFM2 oligonucleotide or si-RNA-A oligonucleotide. Lt, qPCR analysis. Treatment with 60 or 100 nM si-AIFM2 for 24 h or 48 h decreases AIFM2 mRNA expression in SAS cells. Rt, Western blot analysis. Treatment with 100 nM for 24 h si-AIFM2 decreases AIFM2 protein expression in SAS and FaDu cells. (C, D) Wound healing assay and invasion assay, respectively. Knockdown of AIFM2 decreases the competence of wound healing (in C) and invasion (in D) of SAS and FaDu cells. (E) Western blot analysis of the SAS cell. It reveals AKT, ERK, and p38 activation following plasmid transfection for 24 h. The slight upregulation of AIFM2 and COX2 follows the ERK and p38 activation, respectively. Values below the Western blot diagram denote normalized expression levels. oe, transient over-expression. **, and ***, $P < 0.01$, and $P < 0.001$, respectively.

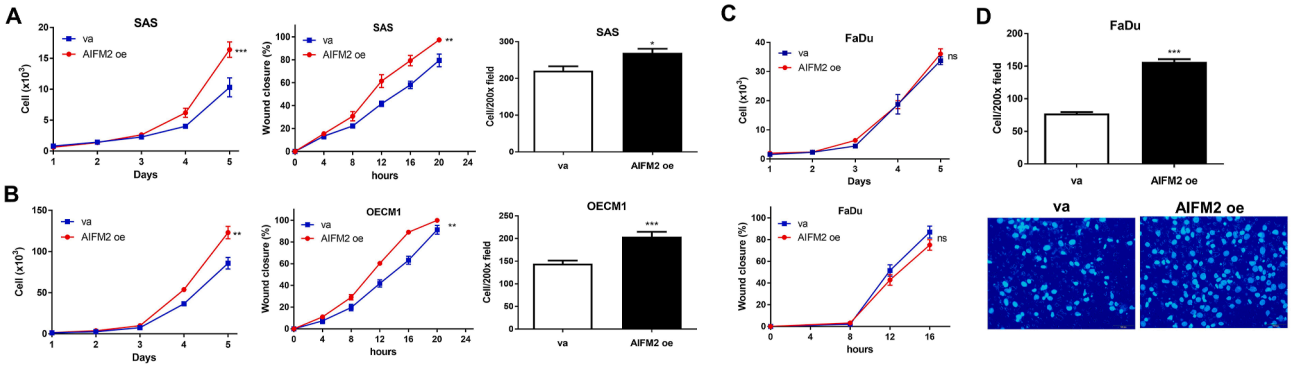

Figure 3 Transient AIFM2 expression in cell lines. (A, B) SAS and OECM1 cells, respectively. Lt, proliferation; middle, wound healing; Rt, invasion. Transient AIFM2 expression increases cell proliferation, wound healing, and invasion. (C, D) FaDu cells. (C) Upper, proliferation. Lower, wound healing. Transient AIFM2 expression does not affect such phenotypes in FaDu cells. (D) Invasion assay. Upper, quantification of invaded cells; Lower, representative fields of invaded cells on the transwell membrane. x200. oe, transient overexpression; va, vector alone. *ns*, not significant. **, and ***, $P < 0.01$, and $P < 0.001$, respectively.

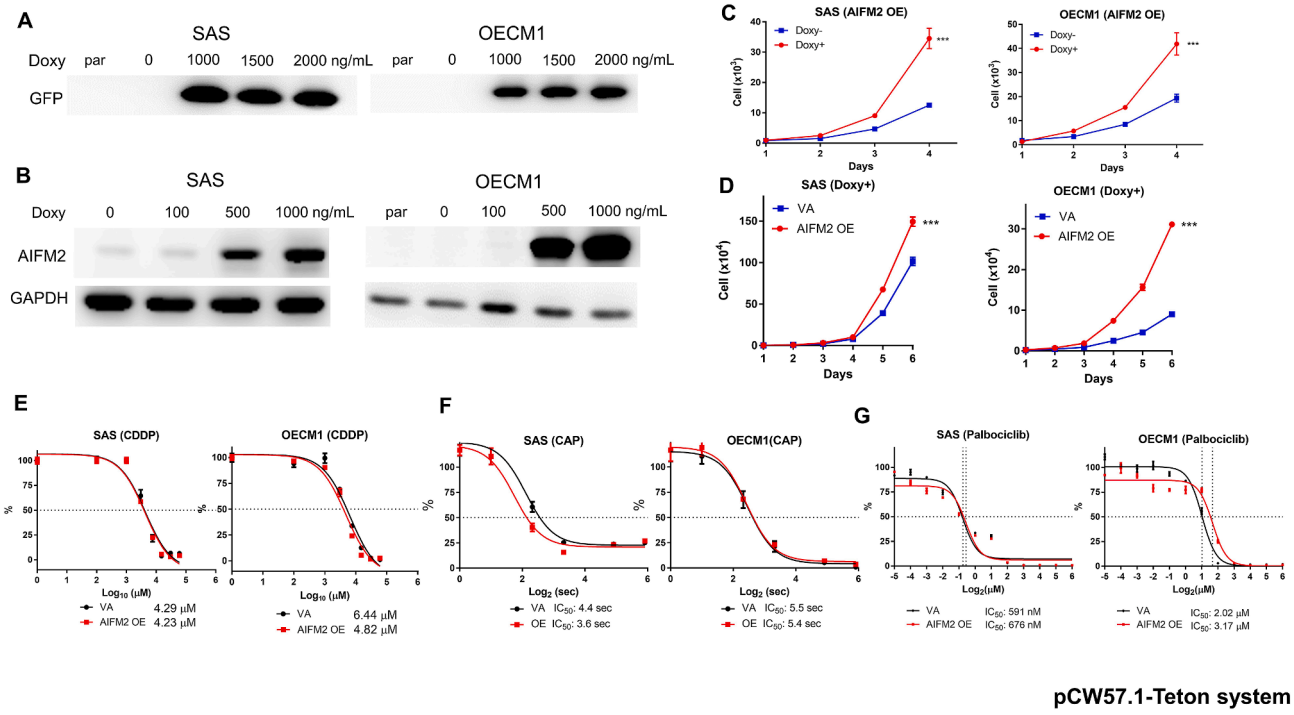

Figure 4 Stable AIFM2 overexpression in cell lines. (A, B) Western blot analysis of SAS and OECM1 cells. (A) GFP OE cell subclones. The Doxy treatments at the doses more than 1000 ng/mL for 48 h drastically induce GFP expression. (B) AIFM2 OE cell subclones. The Doxy treatments at the doses more than 500 ng/mL for 48 h drastically induce AIFM2 expression. (C–G) Lt, SAS cell subclones; Rt, OECM1 cell subclones. (C, D) Proliferation assays. Doxy+, 2000 ng/mL doxycycline treatment for 48 h; Doxy -, no treatment. (C) Comparison between Doxy treatment and control in OE cell subclones. (D) Comparison between OE cell subclones and VA cell subclones in the presence of Doxy treatment. (E–G) Dose response curves of CDDP, CAP, and Palbociclib, respectively. par, parental; OE, stable overexpression; VA, vector alone; CDDP, cisplatin; CAP, cold atmospheric plasma. ***, $P < 0.001$.

tumors compared with lighter smokers or non-smokers. OSCC tumors negative for p16 staining showed increased AIFM2 expression. Importantly, patients whose tumors were within the highest quartile of AIFM2 expression experienced significantly worse survival outcomes compared with those in the lowest quartile (Fig. 1C and D).

Knockdown of AIFM2 decreases the invasiveness of HNSCC/OSCC cell

Compared with NOK cells, six HNSCC cell lines showed elevated AIFM2 mRNA expression, while the OECM1 cell line lacked AIFM2 expression (Fig. 2A). Similar protein analysis

results are shown in the Western blot on the right panel. Knockdown of AIFM2 expression using siRNA in SAS and FaDu cells revealed a decrease in both mRNA and protein expression (Fig. 2B). This is accompanied by a reduction in wound healing and cell invasiveness (Fig. 2C and D). To elucidate the potential upstream regulators, transfection of AKT, ERK, and p38 plasmids activated these three signaling pathways in SAS cells. ERK activation was associated with increased AIFM2 expression (Fig. 2E).

The transient AIFM2 expression increases the oncogenicity

The transient AIFM2 expression mediated by transfection of pcDNA3.1(−) AIFM2 plasmid for 24 significantly increased proliferation (Fig. 3A—Lt), wound healing (Fig. 3A, middle) and invasion (Fig. 3A—Rt) of SAS cells. It also resulted in increased proliferation (Fig. 3B—Lt), wound healing (Fig. 3B, middle) and invasion (Fig. 3B—Rt) of OECM1 cells. However, the transient AIFM2 expression did not affect the proliferation (Fig. 3C, upper) and wound healing (Fig. 3C, lower) of FaDu cells. The transient AIFM2 expression was associated with increased FaDu invasion (Fig. 3D).

The stable AIFM2 expression increases cell growth but does not necessarily affect drug sensitivity

The induction of GFP expression following the treatment of Doxy validated the efficacy of TetOn-GFP plasmid (Fig. 4A). In AIFM2 OE stable cell subclones of SAS and OECM1 carrying TetOn-AIFM2 construct, the treatment with Doxy dosage above 500 ng/mL for 48 h drastically increased AIFM2 protein expression (Fig. 4B). The induced AIFM2 expression mediated by Doxy treatment was associated with increased cell proliferation (Fig. 4C). Following Doxy induction, the increased proliferation in AIFM2 OE cell subclones comparing to VA (carrying TetOn-MCS vector) cell subclones further confirmed that AIFM2 accelerated cell proliferation (Fig. 4D). The survival assays across Doxy-treated AIFM2 OE and VA cell subclones showed that AIFM2 expression drove no or a little sensitizing effect of cells to CDDP (Fig. 4E) and CAP (Fig. 4F) treatments, and a little desensitizing effect to palbociclib treatment (Fig. 4G).

miR-32-5p and miR-432-5p targets AIFM2

miR-150 has been shown to target of AIFM2 on the 3′UTR of the transcript.[25] Analysis using multiple *in silico* modules revealed that miR-150-5p targeted AIFM2, while the targeting of miR-32-5p and miR-432-5p was also predicted by four distinctive modules (Fig. 5A). The 3′UTR of AIFM2 spans ∼1.8 kb. Although miR-150-5p can target site #1881 in the tail part of the 3′UTR sequence,[25,36] algorithms also predict a potential targeting site at #156 in the head part of the 3′UTR (Fig. 5B). We generated head (H) reporter encompassing miR-150-5p, and tail (T) reporter encompassing miR-150-5p site, miR-432-5p and miR-32-5p (Fig. 5B). Following the transfection of Scr and miRNA mimics, the

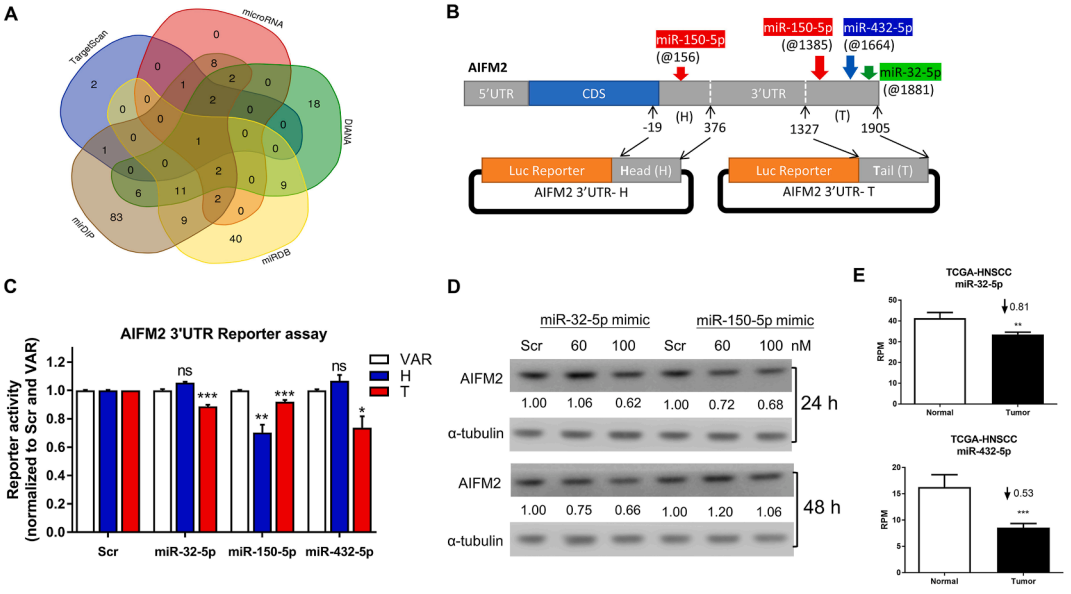

Figure 5 The targeting of suppressor miRNAs on AIFM2. (A) A Venn diagram illustrates the retrieval of potential miRNA repeatedly predicted by 4 or 5 multiple algorithms. (B) Schematic diagram of AIFM2 3′UTR (1905-bp) and the two reporters being constructed to prove the potential targeting of miR-32-5p, miR-150-5p, and miR-432-5p on the AIFM2 3′UTR region. The color boxes and arrows indicate the predicted targeting miRNAs. H and T, the head part and tail part of 3′UTR, respectively. @, the number of the first nucleotide in the binding sites. (C) Reporter assays. Following the treatment of 60 nM miRNA mimics for 24 h, reporter assays are performed to disclose the repression of reporter activity. H, AIFM2 3′UTR-H reporter; T, AIFM2 3′UTR-T reporter; VAR, vector alone reporter. Scr, scramble mimic. Note that miR-150-5p expression represses both H and T reporters, while miR-32-5p and miR-432-5p expression only represses the T reporter. (D) Western blot analysis. The treatment with 100 nM mimics for 24 h represses AIFM2 protein expression. The repression of miR-150-5p mimic lasts to 48 h. Values below the Western blot diagram denote normalized expression levels. (E) miR-32-5p (upper) and miR-432-5p (lower) expression are downregulated in the TCGA HNSCC tumor cohort. RPM, reads per million; Arrows, downregulation. *ns*, not significant. *, **, and ***, $P < 0.05$, $P < 0.01$, and $P < 0.001$, respectively. (For interpretation of the references to color in this figure legend, the reader is referred to the Web version of this article.)

reporter assay was performed. It showed that miR-150-5p expression rendered the decreased H reporter activity. Each miR-32-5p, miR-150-5p, and miR-432-5p expression individually reduced the activity of T reporter (Fig. 5C). The treatment with 100 nM miR-32-5p mimic for 24–48 h decreased AIFM2 protein expression by 30–40 %. The treatment with 100 nM miR-150-5p mimic for 24 h decreased AIFM2 protein expression by 30 % (Fig. 5D). The TCGA HNSCC tumors exhibited the downregulation of miR-32-5p and miR-432-5p (Fig. 5E), and the absence of change in miR-150-5p expression (not shown).

Survival prediction using AIFM2-associated genes

As patients in both the HNSCC and OSCC cohorts with tumors in the highest quartile of AIFM2 expression exhibit worse survival than those in the lowest quartile, we further explore the functional and prognostic implications of this difference using the strategy conceptualized in Fig. 6A. DESeq2 analysis of these expression-defined fractions identifies 2574 protein-coding genes whose expression levels are significantly correlated with AIFM2 in TCGA HNSCC tumors, including 1962 upregulated and 612 downregulated transcripts plotted in volcano plot (Fig. 6B). Using the most stringent analytical criterion (Family-Wise Error Rate; FWER *P*-value) in GSEA, pathways related to ROS regulation, cell proliferation, lipid metabolism, and E2F targets emerge as the most significantly enriched among AIFM2-associated transcripts (Fig. 6C; Table S7; Fig. S1). Additionally, pathways involving PI3K-AKT-mTOR, MYC, and Notch signaling, as well as glycolysis, DNA repair, and the unfolded protein response, are implicated as potential mechanisms underlying AIFM2-related pathogenesis.

Tumor samples are randomly divided into training (60 %) and validation (40 %) cohorts. Further screening with our in-house analytical platform identifies 263 genes significantly associated with patient survival. The top 100 genes with the highest hazard ratios are incorporated into a LightGBM model, which constructs an optimized decision tree that

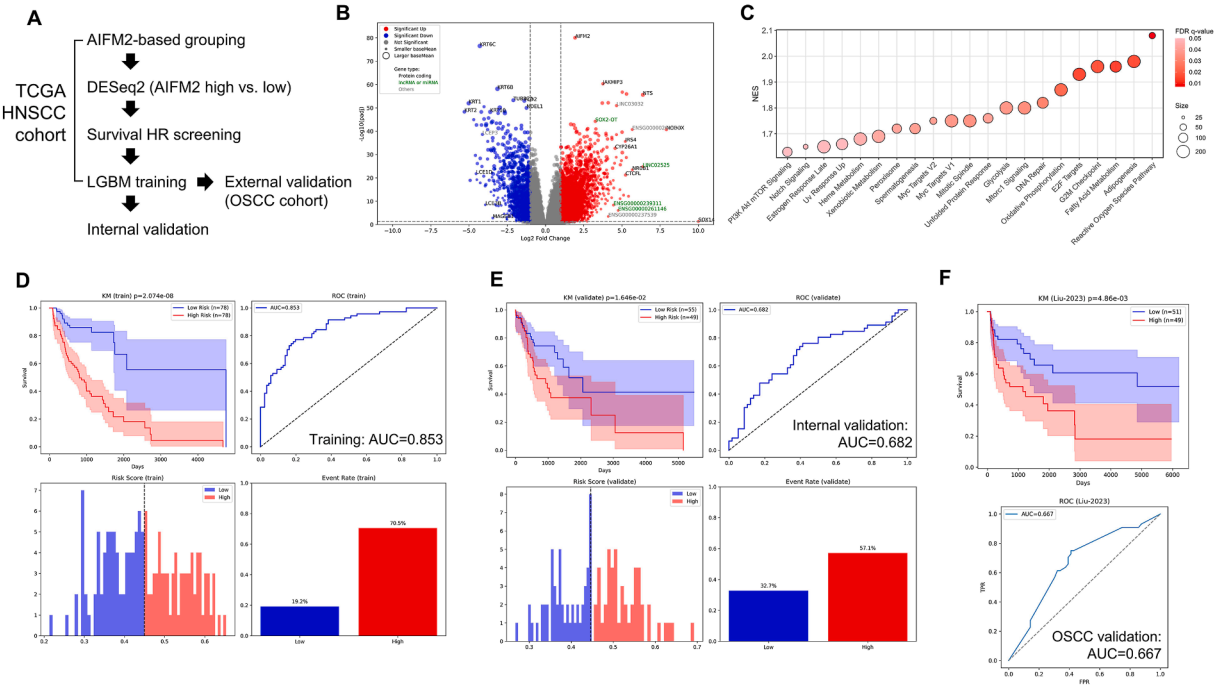

Figure 6 Prediction of patient survival based on the AIFM2-associated gene signature. (A) Schematic illustration of the analytical workflow used for survival prediction. (B) Volcano plot showing significantly dysregulated transcripts correlated with AIFM2 expression in TCGA HNSCC tumors. Red dots indicate upregulated genes, blue dots indicate downregulated genes, and grey dots represent genes without significant change. Representative genes with prominent differential expression are labeled. (C) Bubble plot depicting the major functional pathways enriched among AIFM2-associated transcripts in accordance with Normalized Enrichment Score (NES), False Discovery Rate (FDR)-*q* value and size of hallmarks. Detailed enrichment results are provided in Supplementary Table S7 and Fig. S1. (D, E) Survival analysis of the TCGA HNSCC training cohort (D; $n = 156$) and validation cohort (E; $n = 104$) stratified by risk groups predicted using the Light Gradient Boosting Machine (LGBM) model. Upper left: Kaplan–Meier survival curve; upper right: receiver operating characteristic (ROC) curve; lower left: distribution of risk scores; lower right: event status plot. (F) Survival analysis of the OSCC validation cohort ($n = 100$). Upper panel: Kaplan–Meier survival curve; lower panel: ROC curve. HR, hazard ratio. (For interpretation of the references to color in this figure legend, the reader is referred to the Web version of this article.)

effectively stratifies patients into high- and low-risk groups in the training cohort (*AUC* = 0.853; Fig. 6D). The model retains prognostic performance in both the internal validation (*AUC* = 0.682; Fig. 6E) and OSCC validation cohorts (*AUC* = 0.667; Fig. 6F). We also evaluate the predictive value using the entire HNSCC cohort. DESeq2-derived genes are visualized in a volcano plot (Fig. S2A). HNSCC tumors are divided into training (70 %) and validation (30 %) cohorts. The LightGBM-based model using the selected genes demonstrates strong predictive performance in the training cohort (*AUC* = 0.861; Fig. S2B), with consistent accuracy in the internal validation (*AUC* = 0.691; Fig. S2C) and OSCC validation (*AUC* = 0.660; Fig. S2D) cohorts. Collectively, these results indicate that the AIFM2-associated transcriptional signature provides robust prognostic information for patients with HNSCC and OSCC.

Discussion

In this study, we demonstrated that AIFM2 expression progressively increases with tumor progression in HNSCC and is associated with adverse clinicopathological features of HNSCC/OSCC, including poor differentiation and p16 negativity. Consistently, patients whose tumors exhibited the highest quartile of AIFM2 expression had significantly worse survival outcomes. These findings support the role of AIFM2 as both a marker of tumor aggressiveness and a prognostic biomarker in HNSCC/OSCC.[24,26]

Functionally, our *in vitro* analyses confirmed that AIFM2 promotes tumor cell proliferation, migration, and invasion, as both transient and inducible stable overexpression enhanced oncogenic behaviors in SAS and OECM1 cells. Conversely, AIFM2 knockdown in SAS and FaDu cells suppressed invasiveness, underscoring its contribution to tumor aggressiveness. As the areca or tobacco ingredients stimulate multiple oncogenic signals for neoplastic pathogenesis,[4,40] we explore the potential of signal activation for AIFM2 upregulation. Importantly, ERK activation correlated with AIFM2 upregulation in our preliminary cell studies, suggesting that AIFM2 integrates with canonical oncogenic signaling pathways in OSCC. Although the mechanisms remain to be elucidated, these observations align with studies in hepatocellular carcinoma and drug-resistant tongue carcinoma,[24,26] where AIFM2 has been shown to sustain oncogenicity and metastasis.

Despite its clear oncogenic role, AIFM2 overexpression did not substantially alter therapeutic sensitivity in our stable cell models, with only modest effects observed for cisplatin, palbociclib, and cold atmospheric plasma. This suggests that while AIFM2 accelerates tumor progression, its role in therapy resistance may be context-dependent or compensated by parallel survival pathways. Previous work has shown that AIFM2 suppresses ferroptosis and contributes to therapy resistance in various cancers.[18–21] Therefore, additional investigations are warranted to determine whether HNSCC/OSCC harbor specific ferroptotic vulnerabilities that could be therapeutically exploited by targeting AIFM2.

We further identified miR-32-5p and miR-432-5p as tumor-suppressive regulators of AIFM2 in HNSCC/OSCC. Both miRNAs were significantly downregulated in tumors, and luciferase reporter assays confirmed their direct binding to the AIFM2 3′UTR. Restoration of these miRNAs reduced AIFM2 protein expression, highlighting a potential therapeutic axis. Given that dysregulation of tumor-suppressive miRNAs is widespread in OSCC,[3,13,31–34] strategies aimed at restoring their expression may represent a rational approach to mitigate AIFM2-driven oncogenicity.

Our findings establish a comprehensive analytical framework linking AIFM2-associated gene expression to signal activation or patient prognosis in HNSCC/OSCC. AIFM2-correlated transcripts were significantly enriched in pathways related to oxidative stress, proliferation, lipid metabolism, and cell death, consistent with our results in clinical assessment and functional assay, and previous studies.[9,11,16,18,19,21,27] However, the versatile roles of AIFM2 in modulating crucial signals during tumorigenesis such as mTOR, MYC, and Notch warrant further investigation. Using a machine learning, we effectively stratified patients into high- and low-risk groups with strong predictive accuracy in the training cohort.[39] Although the model's performance declined slightly in the validation cohorts, it maintained meaningful prognostic value. These results suggest that this analytical module could facilitate clinical risk stratification in additional HNSCC/OSCC cohorts.

This study may have several limitations. First, although our *in vitro* data strongly support the oncogenic role of AIFM2, *in vivo* validation using xenograft or genetically engineered models is required to confirm its relevance in tumor initiation and progression. Second, while we identified miR-32-5p and miR-432-5p as regulators, other epigenetic mechanisms or upstream oncogenic signals may also contribute to AIFM2 dysregulation.[15,23,25] Finally, the modest influence of AIFM2 on therapy resistance suggests that combinatorial targeting of ferroptosis pathways may be necessary to achieve meaningful therapeutic benefit. Collectively, our findings indicate that the AIFM2-associated gene signature represents a promising biomarker for prognostic assessment in HNSCC/OSCC.

This study provides evidence that AIFM2 acts as a key oncogenic driver in HNSCC and OSCC, promoting tumor progression while being epigenetically regulated by suppressor miRNAs. These findings underscore the dual potential of AIFM2 as both a prognostic biomarker and a therapeutic target. Future studies should explore the translational potential of targeting AIFM2 or restoring its regulatory miRNAs as strategies to improve clinical outcomes in HNSCC/OSCC patients.

Declaration of competing interest

The authors have no conflicts of interest relevant to this article.

Acknowledgements

The authors would like to acknowledge the assistance of Professors Shou-Yen Kao and Hsi-Feng Tu, as well as Messrs. Jian-Hua Pan and Chun-Yu Fan-Chiang. This study was supported by grants 111-2314-B-A49-025-MY3, 113-2811-B-A49A-047, 114-2811-B-A49A-002, and 114-2811-B-A49A-019

(postdoctoral training grant for Chou C.H.) from the National Science and Technology Council (NSTC), Taiwan.

Appendix A. Supplementary data

Supplementary data to this article can be found online at https://doi.org/10.1016/j.jds.2025.11.007.

References

1. Chou CH, Tu HF, Kao SY, et al. Targeting of miR-31/96/182 to the numb gene during head and neck oncogenesis. *Head Neck* 2018;40:808—17.
2. Liu CJ, Tsai MM, Hung PS, et al. miR-31 ablates expression of the HIF regulatory factor FIH to activate the HIF pathway in head and neck carcinoma. *Cancer Res* 2010;70:1635—44.
3. Chou CH, Yen CH, Liu CJ, Tu HF, Lin SC, Chang KW. The upregulation of VGF enhances the progression of oral squamous carcinoma. *Cancer Cell Int* 2024;24:115.
4. Lu HH, Kao SY, Liu TY, et al. Areca nut extract induced oxidative stress and upregulated hypoxia inducing factor leading to autophagy in oral cancer cells. *Autophagy* 2010;6:725—37.
5. Dixon SJ, Lemberg KM, Lamprecht MR, et al. Ferroptosis: an iron-dependent form of nonapoptotic cell death. *Cell* 2012;149:1060—72.
6. Hadian K, Stockwell BR. SnapShot: ferroptosis. *Cell* 2020;181:1188—1188e1.
7. Yang WS, SriRamaratnam R, Welsch ME. Regulation of ferroptotic cancer cell death by GPX4. *Cell* 2014;156:317—31.
8. Wu Y, Yu C, Luo M, et al. Ferroptosis in cancer treatment: another way to Rome. *Front Oncol* 2020;10:571127.
9. Stockwell BR, Friedmann Angeli JP, Bayir H, et al. Ferroptosis: a regulated cell death nexus linking metabolism, redox biology, and disease. *Cell* 2017;171:273—85.
10. Kennedy L, Sandhu JK, Harper ME, Cuperlovic-Culf M. Role of glutathione in cancer: from mechanisms to therapies. *Biomolecules* 2020;10:1429.
11. Pope LE, Dixon SJ. Regulation of ferroptosis by lipid metabolism. *Trends Cell Biol* 2023;33:1077—87.
12. Chen Z, Cai H, Ye W, et al. TP63 transcriptionally regulates SLC7A5 to suppress ferroptosis in head and neck squamous cell carcinoma. *Front Immunol* 2024;15:1445472.
13. Liu YC, Liu SY, Lin YC, Liu CJ, Chang KW, Lin SC. The disruption of NEAT1-miR-125b-5p-SLC1A5 cascade defines the oncogenicity and differential immune profile in head and neck squamous cell carcinoma. *Cell Death Discov* 2024;10:392.
14. Cheng YC, Chang KW, Pan JH, et al. Cold atmospheric plasma jet irradiation decreases the survival and the expression of oncogenic miRNAs of oral carcinoma cells. *Int J Mol Sci* 2023;24:16662.
15. Zhang Y, Xu Z, Wen W, et al. The microRNA-3622 family at the 8p21 locus exerts oncogenic effects by regulating the p53-downstream gene network in prostate cancer progression. *Oncogene* 2022;41:3186—96.
16. Lu J, Chen J, Xu N, et al. Activation of AIFM2 enhances apoptosis of human lung cancer cells undergoing toxicological stress. *Toxicol Lett* 2016;258:227—36.
17. Gong M, Hay S, Marshall KR, Munro AW, Scrutton NS. DNA binding suppresses human AIF-M2 activity and provides a connection between redox chemistry, reactive oxygen species, and apoptosis. *J Biol Chem* 2007;282:30331—40.
18. Bersuker K, Hendricks JM, Li Z, et al. The CoQ oxidoreductase FSP1 acts parallel to GPX4 to inhibit ferroptosis. *Nature* 2019;575:688—92.
19. Doll S, Freitas FP, Shah R, et al. FSP1 is a glutathione-independent ferroptosis suppressor. *Nature* 2019;575:693—8.
20. Tahsin T, McPhail DK, Champion JD, et al. Targeting NRF2 and FSP1 to overcome ferroptosis resistance in TSC2-deficient and cancer cells. *Cancers (Basel)* 2025;17:2714.
21. Roh JL. Targeting ferroptosis suppressor protein 1 in cancer therapy: implications and perspectives, with emphasis on head and neck cancer. *Crit Rev Oncol Hematol* 2024;202:104440.
22. Pei W, Jiang M, Liu H, Song J, Hu J. The prognostic and antitumor roles of key genes of ferroptosis in liver hepatocellular cancer and stomach adenocarcinoma. *Cancer Biomarkers* 2024;39:335—47.
23. Bazhabayi M, Qiu X, Li X, et al. circGFRA1 facilitates the malignant progression of HER-2-positive breast cancer through acting as a sponge of miR-1228 and enhancing AIFM2 expression. *J Cell Mol Med* 2021;25:10248—56.
24. Guo S, Li F, Liang Y, et al. AIFM2 promotes hepatocellular carcinoma metastasis by enhancing mitochondrial biogenesis through activation of SIRT1/PGC-1 alpha signaling. *Oncogenesis* 2023;12:46.
25. Wang G, Yao Y, Xie J, Wen C. Long noncoding RNA ZFAS1 exerts a suppressive impact on ferroptosis by modulating the miR-150/AIFM2 axis in hepatocellular carcinoma cells. *Heliyon* 2024;10:e37225.
26. Wu YC, Huang CS, Hsieh MS, et al. Targeting of FSP1 regulates iron homeostasis in drug-tolerant persister head and neck cancer cells through lipid-metabolism-driven ferroptosis. *Aging (Albany NY)* 2024;16:627—47.
27. Peng W, Liang J, Qian X, Li M, Nie M, Chen B. IGF2BP1/AIFM2 axis regulates ferroptosis and glycolysis to drive hepatocellular carcinoma progression. *Cell Signal* 2025;130:111660.
28. Chen YF, Yang CC, Kao SY, Liu CJ, Lin SC, Chang KW. MicroRNA-211 enhances the oncogenicity of carcinogen-induced oral carcinoma by repressing TCF12 and increasing antioxidant activity. *Cancer Res* 2016;76:4872—86.
29. Li CX, Su Y, Wang ZY, Liu H, Gong ZC, Zhao HR. A PRISMA meta-analysis for diagnostic value of microRNA-21 in head and neck squamous cell carcinoma along with bioinformatics research. *Oral Maxillofac Surg* 2024;28:739—52.
30. Dioguardi M, Spirito F, Sovereto D, et al. The prognostic role of miR-31 in head and neck squamous cell carcinoma: systematic review and meta-analysis with trial sequential analysis. *Int J Environ Res Publ Health* 2022;19:5334.
31. Dioguardi M, Musella G, Bizzoca ME, et al. The prognostic role of miR-375 in head and neck squamous cell carcinoma: a systematic review, meta-analysis, and trial sequential analysis. *Int J Mol Sci* 2025;26:2183.
32. Dioguardi M, Spirito F, Iacovelli G, et al. The potential microRNA prognostic signature in HNSCCs: a systematic review. *Noncoding RNA* 2023;9:54.
33. Malekjafarian SM, Mohtasham N, Mirhashemi M, et al. Metastasis and cell proliferation inhibition by microRNAs and its potential therapeutic applications in OSCC: a systematic review. *Pathol Res Pract* 2024;262:155532.
34. Yu M, Cao H, Yang J, Liu T, Gao J, Wong B. EIF4A3-regulated hsa_circ_0001445 can inhibit the progression of laryngeal squamous cell carcinoma through hsa-miR-432-5p-dependent up-regulation of RGMA expression. *Cell Cycle* 2023;22:2038—56.
35. Citron F, Armenia J, Franchin G, et al. An integrated approach identifies mediators of local recurrence in head and neck squamous carcinoma. *Clin Cancer Res* 2017;23:3769—80.
36. Huang J, Xu Y, Huang P. Salivary miR-150-5p as an indicator of periodontitis severity and regulator of human periodontal ligament fibroblast behavior by targeting AIFM2. *J Periodontal Res* 2024;59:187—94.
37. Chang KW, Hung WW, Chou CH, et al. LncRNA MIR31HG drives oncogenicity by inhibiting the limb-bud and heart development gene (LBH) during oral carcinoma. *Int J Mol Sci* 2021;22:8383.

38. Chang SR, Chou CH, Tu HF, Liu CJ, Chang KW, Lin SC. The expression of immune co-stimulators as a prognostic predictor of head and neck squamous cell carcinomas and oral squamous cell carcinomas. *J Dent Sci* 2024;19:1380—8.
39. Alabi RO, Elmusrati M, Leivo I, Almangush A, Makitie AA. Collaborative machine learning-guided overall survival prediction of oral squamous cell carcinoma. *Acta Otolaryngol* 2024;188:105464.
40. Feng C, Mao W, Yuan C, Dong P, Liu Y. Nicotine-induced CHRNA5 activation modulates CES1 expression, impacting head and neck squamous cell carcinoma recurrence and metastasis through MEK/ERK pathway. *Cell Death Dis* 2024;15:785.